Molecular Simulations of Hydrated Proton Exchange Membranes: the Structure

Gabriel Marchand[a,b], Philippe A. Bopp[b], and Eckhard Spohr[a]

[a] Lehrstuhl für Theoretische Chemie, Fakultät für Chemie, Universität Duisburg-Essen, Campus Essen (S05 V06 E15), Universitätsstraße 5, DE-45141 Essen

[b] Department of Chemistry, Université de Bordeaux, 351 Cours de la Libération Bât A12, FR-33405 Talence CEDEX

Reprint requests to P. A. B.; E-mail: philippebopp@yahoo.com

Z. Naturforsch. **68a,** 101 – 111 (2013) / DOI: 10.5560/ZNA.2012-0089
Received September 27, 2012 / published online February 15, 2013

Dedicated to Professor Alfred Klemm on the occasion of his 100th birthday

The structure of two hydrated proton exchange membranes for fuel cells (PEMFC), Nafion® (Dupont) and Hyflon® (Solvay), is studied by all-atom molecular dynamics (MD) computer simulations. Since the characteristic times of these systems are long compared to the times for which they can be simulated, several different, but equivalent, initial configurations with a large degree of randomness are generated for different water contents and then equilibrated and simulated in parallel. A more constrained structure, analog to the newest model proposed in the literature based on scattering experiments, is investigated in the same way. One might speculate that a limited degree of entanglement of the polymer chains is a key feature of the structures showing the best agreement with experiment. Nevertheless, the overall conclusion remains that the scattering experiments cannot distinguish between the several, in our view equally plausible, structural models.

We thus find that the characteristic features of experimental scattering curves are, after equilibration, fairly well reproduced by all systems prepared with our method. We thus study in more detail some structural details. We attempt to characterize the spatial and size distribution of the water rich domains, which is where the proton diffusion mostly takes place, using several clustering algorithms.

Key words: Molecular Dynamics; Nafion; Equilibration; Structure; Clustering.
PACS numbers: 61.20Gy; 61.20Ja; 61.20.Qg; 61.25.H-

1. Introduction and Review

Molecular dynamics (MD) computer simulations, which were pioneered in Europe in the 1970ies by Schäfer and Klemm [1] for molten salts and by Heinzinger and Vogel [2] for aqueous ionic solutions (among others), have become an almost universal tool for the investigation of condensed phases, be they homogeneous or heterogeneous. We apply here this method to particular challenging systems: Nafion and Hyflon, two hydrated proton exchange membranes for fuel cells (PEMFC) [3].

Compared to other electrical energy conversion devices, the main advantage of fuel cells is the high energy-to-mass ratio that can be achieved. All fuel cells are based on the same principle: energy from chemical reactions is converted into electrical energy, producing direct current electricity, which is fed to an external circuit. For the so-called low- and intermediate-temperature fuel cells (those favoured in the automotive industry), proton-conducting materials are used as the electrolyte. Nafion and Hyflon ionomers have been considered to be the reference proton-conducting material with which most experimental and theoretical studies have been compared.

These two ionomers are composed of a CF_2-backbone with pendant sulfonated side chains, which are able to induce, in the presence of water or other hydrophilic solvents, an hydrophobic/hydrophilic phase separation at the nanometer scale [4, 5]. It is within the aqueous domains that ionic conductivity occurs. Compared to Nafion, the Hyflon molecules have shorter side chains. Experimentally, the major difference between Hyflon and Nafion is the higher glass-transition temperature in Hyflon.

When increasing the water content, the membrane swells. The connectivity between the hydrophilic domains increases until a single interconnected large domain appears, i. e., until the threshold to water percolation is reached [3, 4, 6 – 19]. In this case, the membrane conductivity rapidly increases with increasing water content. Protons dissociate from the SO_3^--groups and are shuttled through the hydrogen bond network, e. g. via the Grotthuss structural diffusion mechanism, which continuously breaks and reforms bonds between protons and water molecules (see, e. g., [20 – 29]). Such a shuttling mechanism was first suggested by Grotthuss in 1806 [30], subsequently revisited many times, e. g., in 1995 [31], and further elaborated on the basis of ab initio MD simulations [32, 33].

Even though this picture is generally accepted, a debate concerning the exact nanoscale morphology persists, in particular since unambiguous experiments are missing. The numerous scattering data collected over the last years using a variety of scattering methods did not provide an unambiguous answer. Morphological models involving specific assumptions are needed for their interpretation. Numerous such models have thus been proposed, ranging from the historical hard-sphere model of Gierke et al. [5] to, for instance, the more recent 'parallel cylindrical water nanochannel' picture by Schmidt-Rohr and Chen [34]. For many reasons, none of these efforts has led to an entirely satisfactory picture.

The investigation of such morphologies via molecular simulations remains challenging since it requires very large systems and very long simulations. The systems should be large enough to include several of these hydrophilic domains. This is difficult and most of the simulation studies in the literature (see e. g. [10, 20, 21, 35 – 41]) focused on the proton transfer process assuming more or less fixed structures for the polymer at small and intermediate length scales (typically up to a few nanometers).

Several studies have attempted to characterize the morphologies of hydrated Nafion membranes in various other ways (see e. g. [42 – 46]). Wescott et al. [45], for example, performed mesoscale simulations of hydrated Nafion using a self-consistent mean field theory approach and a coarse-grained model, deriving the interaction parameters from classical MD. In this study, four systems (with different water contents) with an initially homogeneous distribution of the components were simulated at room temperature. The simulations at lower water contents led to isolated, nearly spherical domains. At higher water contents, the domains had more elliptical or barbell shapes due to domain merging. Also, percolation was observed at the highest water contents. A recent series of dissipative particle dynamics (DPD) simulations [47, 48] extended the range of studies on polymer morphology to characteristic lengths of almost 100 nm. The expected fluorocarbon crystallites were, however, not seen. Again, either isolated water clusters or a continuous water domain were observed, depending on the hydration level.

In 2010, the nanoscale morphology of six models of Nafion was investigated by Knox and Voth [18] via large-scale computer simulations: a few nanoseconds with two million atoms in $30 \times 30 \times 30\ \mathrm{nm}^3$ boxes. Except for their 'random model', all models were found to exhibit scattering profiles in agreement with experiment, in spite of their very different initial geometries. The fact that their random structure did not reproduce the experimental scattering data is most likely due to a high initial degree of entanglement of the polymer chains. Considering the very long time scales for the processes involved in the polymer motions, these authors stated that, given sufficient time, the random model would also reproduce the scattering profile, 'although the time scale for such peak formation is not computationally feasible'.

In this work, we propose a new random morphological model of Nafion/Hyflon, similar to, but different from, the one proposed by Knox and Voth [18]. We have tried to generate the polymer chains with as few external constraints as possible (i. e. except the ones inherent in their molecular structures and the ones imposed by the required periodicity) and thus limit their entanglement. Since this is our first communication on these systems, the procedure to generate the initial conditions for the simulations will be described in some detail in the next section. In total, 13 systems have been equilibrated and simulated over times in the range from 15 to 40 nanoseconds, see Table 1. We compare the structures obtained with this model to ones obtained with a 'cylindrical' model similar to the newest experimental model [34]. The total structure factors $S(Q)$ have been computed, and here we compare the X-ray weighted $S(Q)$ with experimentally obtained scattering profiles available in the literature. The structure of the aqueous domains is further characterized by means of cluster analyses.

Table 1. Simulated systems.

System	Ionomer	λ	# atoms	t_{sim} [ns]	name*
1	Nafion	10	396000	41.5	NR-10-1
2	Nafion	10	396000	25.2	NR-10-2
3	Nafion	10	396000	23.5	NR-10-3
4	Nafion	10	396000	25.2	NR-10-4
5	Nafion	10	396000	23.3	NR-10-5
6	Nafion	10	396000	25.1	NR-10-6
7	Nafion	7.5	366000	15.0	NR-7.5-1
8	Nafion	7.5	366000	15.0	NR-7.5-2
9	Nafion	5	336000	15.0	NR-5-1
10	Nafion	5	336000	15.0	NR-5-2
11	Nafion	10	427680	15.6	NC-10-1
12	Hyflon	10	356000	23.9	HR-10-1
13	Hyflon	10	356000	22.5	HR-10-2

* N = Nafion, H = Hyflon; R = 'random' initial geometry, C = 'cylindrical' initial geometry. All systems except the 'cylindrical' one (NC-10-1) have 'random' initial geometries; t_{sim} is the total simulation time of the run.

2. System Setup

In order to avoid, as far as possible, any bias, we have chosen to generate several mesoscopically equivalent, but microscopically different (with different atomic positions), initial conditions with as much randomness as possible. We use two types of geometrical constraints at the level of the simulation box: none (systems called 'random') and some excluded volumes (systems called 'cylindrical'). We also investigate the effect of changing the water content ($\lambda = 5$, 7.5, and 10, where λ is the number of water molecules per sulfonate group) and the side chain length (Nafion/Hyflon). We then simulate these systems, first reducing their sizes until the approximate equilibrium density is reached and then observe whether the resulting structures are compatible with the available experimental information. Since this is found to be the case, we study the so-generated structures.

2.1. 'Random' Model

The general setup procedure is summarized in Table 2. The initial geometries of the polymer chains were generated by random walk processes subject to several constraints. The guiding principle was to grow the polymer chains with as few constraints as possible and thus limit their entanglement. We thus assumed a-priori a larger available volume for the chains (see below) than the one of the final simulation box, which corresponds to the equilibrium density of the system at the desired temperature. Each chain had a unique random starting point and a unique random path. The N desired chains were thus grown sequentially in the

Table 2. Setup of the systems.

step		number density	time
	NR and HR systems		
1	build polymer chains in large[i] box	below experimental	–
2	relax[ii] polymer chains	–	0.5 ns
3	add water for λ=10	below experimental	–
4	relax the whole system[iii]	–	–
5	run in NpT-simulations	converging toward experiment[iv]	1 – 6 ns[v]
6	collect data in NpT-'equilibrium'	stationary $\pm < 1\%$	13 – 40 ns
7	for $\lambda < 10$ remove water randomly from last configuration and go back to 5		
	NC system		
1	build polymer chains in box[vi]	$\approx$ experimental	–
2	relax polymer chains[iii]	–	–
3	add water	$\approx$ experimental	–
4	relax the whole system[iii]	–	–
5	run in NpT-simulations	stationary $\pm < 1\%$	1 ns
6	collect data in NpT-'equilibrium'	stationary $\pm < 1\%$	14.6 ns

[i] $20 \times 20 \times 20$ nm^3 for Nafion, $30 \times 30 \times 30$ nm^3 for Hyflon;
[ii] standard energy minimization (steepest descent algorithm) and 0.5 ns of NpT ($p = 1$ bar, $T = 300$ K) simulation;
[iii] energy minimization only;
[iv] overall change in density: 20% for Nafion, 80% for Hyflon;
[v] 1 – 2 ns for Nafion, 6 ns for Hyflon;
[vi] outside of 'empty cylinders'.

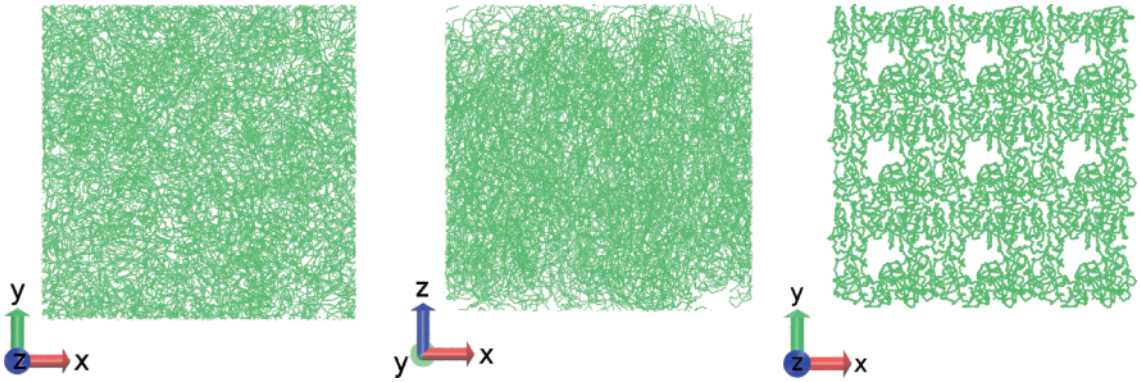

Fig. 1 (colour online). Polymer chains at the beginning of the simulations. Left and middle panels: two orthographic projections of an NR-10 system, right panel: the NC-10-1 system seen along the z-axis. The x, y, and z-axes are shown at the bottom left. Only the C-atoms of the backbone are shown.

large volume. Starting the simulation from a very low density (i. e. a too big box) would require excessively long simulation times or extreme compression rates to reach the proper density. Such a procedure could possibly also lead to semicrystalline morphologies, which we did not intend to study in the present context. A compromise must thus be found between the ease of growing the chains and the duration of the subsequent approach to equilibrium.

In contrast to the study by Knox and Voth [18], we did not consider the randomness of the comonomeric sequence: the side chains were periodically separated by 15 CF_2-groups. It corresponds to an equivalent weight of about $1150\,\mathrm{g \cdot mol^{-1}}$. In the language of Jang et al. [49] who studied the effect of the monomeric sequence on the structure of Nafion and which suggested a certain influence on the nanophase segregation, our model corresponds to what they call the 'dispersed' sequence.

The setup process (Tab. 2) is described in more detail in the appendix; Figure 1 gives a visual impression of the structure of the so obtained systems. One sees domains with mostly extended polymer chains, where the density of water molecules and ions is low (white regions). Except for the cylindrical case, no particular global structure is seen.

2.2. 'Cylindrical' Model

In addition to the 'random' model, we studied a model similar to the one proposed by Schmidt-Rohr and Chen [34]. In contrast to the picture put forward by these authors, i. e. the existence of domains where the water density is strictly zero, we distributed the water molecules and counterions inside and outside predefined cylindrical volumes with a low density outside and a high density inside these volumes. In contrast to the random model, we initiated the cylindrical system at a density close to the experimental one: starting the simulation from a low density might have destroyed the initial cylindrical structure during the 'compression'.

We first placed 8 Nafion chains in a $6 \times 6 \times 6\,\mathrm{nm}^3$ box with the same growth algorithm as for the random systems (see appendix), but with the additional constraint that the backbone of the polymer was not allowed to approach closer than a value $r_{\mathrm{cyl}} = 1.5\,\mathrm{nm}$ (the radius of the cylinder along the z-direction) to the center of this box. The polymer density of this small system was then $\approx 1406\,\mathrm{kg \cdot m^{-3}}$. According to the model by Schmidt–Rohr and Chen [34], the water channels had diameters of between 1.8 and 3.5 nm with an average of 2.4 nm. This small system was then submitted to a standard energy minimization and replicated in the x-, y-, and z-directions in order to construct a large system, see also Table 2.

The system was then filled with water ($\lambda = 10$), leading to a total density of $\approx 1675\,\mathrm{kg \cdot m^{-3}}$. In average, $\approx 40\%$ of the water molecules and $\approx 34\%$ of the K^+-ions are found initially inside the channels, which leads to a local density of the water molecules and K^+-ions of $\approx 423\,\mathrm{kg \cdot m^{-3}}$, while the density (of water molecules and K^+-ions) in the whole volume is $\approx 269\,\mathrm{kg \cdot m^{-3}}$. This system is also shown in Figure 1.

3. Interaction Model

We used an all-atom representation for the potential energy of the polymer and the solvent,

$$V^{\text{tot}} = V^{\text{inter}} + V^{\text{intra}}, \tag{1}$$

where V^{inter} refers to the intermolecular terms between polymer chains (also the so-called non-bonded term within a polymer strand), between polymer and water, and between water molecules (simple point charge (SPC) model [50]). V^{intra} refers to the other intramolecular interactions of the polymer, the water molecules being rigid.

V^{inter} consists in the usual fashion of sums of electrostatic Coulomb potential terms between partial charges located at the atoms and of Lennard–Jones terms between these sites. V^{intra} is written in terms of bond stretches $(r - r_0)$ and the deformations of planar (θ) and dihedral (ϕ) angles:

$$\begin{aligned} V^{\text{intra}} = & \sum_{\text{bonds}} \left(\frac{k_r}{2} (r - r_0)^2 \right) \\ & + \sum_{\text{angles}} \left(\frac{k_\theta}{2} (\cos\theta - \cos\theta_0)^2 \right) \\ & + \sum_{\text{torsions}} \left(\frac{k_\phi}{2} \{1 - \cos[3(\phi - \pi)]\} \right), \end{aligned} \tag{2}$$

where the sums are taken over all internal coordinates of a given type; k_r stands for the various stretching force constants, k_θ are the bending force constants, and k_ϕ is the torsion force constant for any dihedral angle between the three first and the three last bonded atoms. r_0 and θ_0 denote equilibrium distances and angles, respectively. All force field parameters were taken from the literature [50–52] and can also be found in [53].

In many simulations studies of Nafion [18, 35, 36, 49, 54, 55], a modified version of the DREIDING force field [49, 56, 57] was used together with the flexible three-centered (F3C) water model and an explicit hydronium model [49, 58]. This combination was found to reproduce the experimental density satisfactorily [18]. As seen above this is also true for the present force field, which also reproduces the frequency range of the vibrational modes in Nafion and Hyflon satisfactorily. A difference to other Nafion force fields is that there are no partial electric charges on the carbon (C), fluorine (F), and ether oxygen (Oe) atoms. Only the sulfur (S) and the sulfur oxygens (Os) carry such charges.

4. Molecular Dynamics Simulations

The simulations were performed in the NpT-ensemble at 1 bar and 300 K with the GROMACS [59] program package. The Berendsen thermostat [60] and barostat [60] were used with a coupling time constant of 1 ps for both the thermostat and the barostat to keep the temperature and pressure constant. Orthorhombic periodic boundary conditions (PBC) were applied; the integration time step was 2.0 fs. For the long-range interactions, we employed the particle mesh Ewald method [61, 62] with a mesh spacing of 1.2 Å. The short-range interactions were truncated beyond a cut-off distance $r_c = 10$ Å using the shifted-force method. The trajectory was recorded for further analysis every 5000 steps (i. e. every 10 ps).

Altogether 13 systems, different either by their water contents, their initial geometries, or their side chain lengths were simulated, see Table 1. The 6 first Nafion systems had equivalent (random) initial geometries and water contents ($\lambda = 10$), they differed only in the initial positions of the atoms. The nomenclature (last column of Tab. 1) to identify our systems is described in the table caption.

Except for the system NC-10-1 (see Tab. 1), each system was composed of 200 polymer chains (each containing 20 side chains): there were thus 4000 SO_3-groups and as many K^+-ions. Depending on the water content, there were between 20000 ($\lambda = 5$) and 40000 water molecules ($\lambda = 10$) in the system. NC-10-1, on the other hand, contained 216 polymer chains, hence 4320 (216*20) SO_3^--groups, 4320 K^+, and 43200 H_2O.

5. The Structure of Hydrated Nafion and Hyflon

5.1. Scattering Function $S(Q)$

One way to compare the simulated structure with experimental data is to calculate the so-called total structure factor $S(Q)$, which is obtained e. g. from X-ray or neutron scattering, from the simulations. For Nafion and Hyflon systems, a peak in $S(Q)$ is usually observed in both cases at $Q \approx 0.1 - 0.15$ Å^{-1} [4, 63–66], depending on the water content. It is called the ionomer peak and this periodicity of the contrast is usually interpreted as resulting from a mean separation distance between aqueous clusters of $2\pi/Q \approx 4 - 6$ nm. This peak shifts to lower Q-values (longer

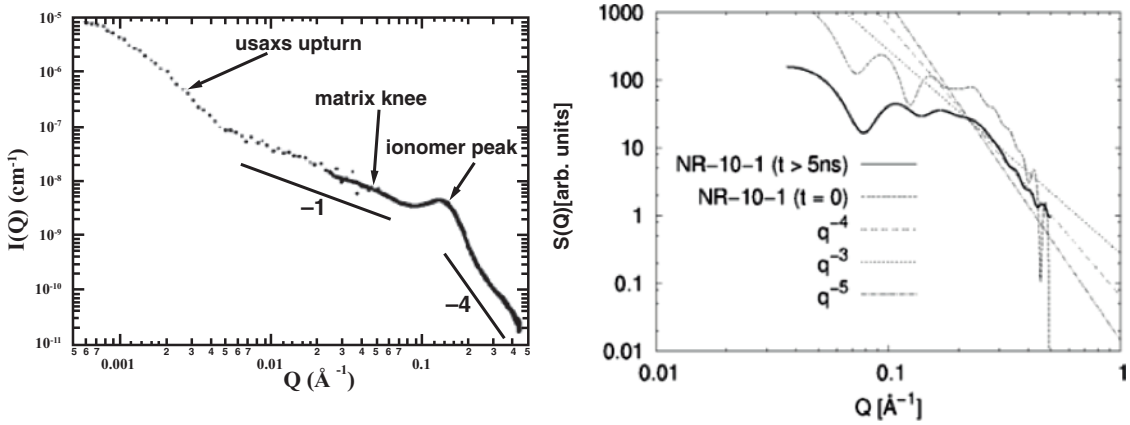

Fig. 2. Left: log–log representation of the small-angle X-ray scattering curve [64]; right: simulations using the 'random' model: after equilibration (full line); during equilibration (i. e. at a slightly lower density) for comparison (dashed line). The straight lines in the right frame are various power law fits to the curve after equilibration in the region $0.2\,\text{Å}^{-1} < Q < 0.5\,\text{Å}^{-1}$.

distances) as the water content increases. Also, there is a broad, lower Q ($\approx 0.03\,\text{Å}^{-1}$) region ('matrix knee') that has been assigned to semicrystalline polymer regions and a smooth 'Porod region' at higher Q ($\approx 0.3\,\text{Å}^{-1}$), where the intensity is expected to decay obeying a q^{-4} power law [4, 64]. Treating the 'matrix knee' region via atomistic computer simulation would require much larger simulation boxes than the ones in this study, which is currently not an option.

Figure 2 shows a typical experimental scattering profile of a Nafion membrane soaked in water obtained from small angle X-ray scattering (SAXS) and ultra SAXS (USAXS) measurements [64], together with the computed (X-ray weighted) $S(Q)$-profiles of NR-10-1 before and after step 6 in Table 2. We considered here only the region $Q > 0.08\,\text{Å}^{-1}$. At the end, the computed scattering profile of this 'random' system was consistent with the experimental one, while it was not so for the starting configurations (during step 5). This system (and the others as well) was thus correctly evolving toward a structure compatible with experiment: both the ionomer peak around $0.1\,\text{Å}^{-1}$ and, as the fits show, the q^{-4} power law decay, were evident. A more detailed analysis shows that $S(Q)$ becomes stationary for $t \gtrsim 5$ ns for all systems. The same conclusions can be drawn from the neutron-weighted curves, which are not shown here.

Figure 3 shows the variations between $S(Q)$ of the various NR-10 runs and between the averages obtained for different systems. A peak akin to the ionomer peak

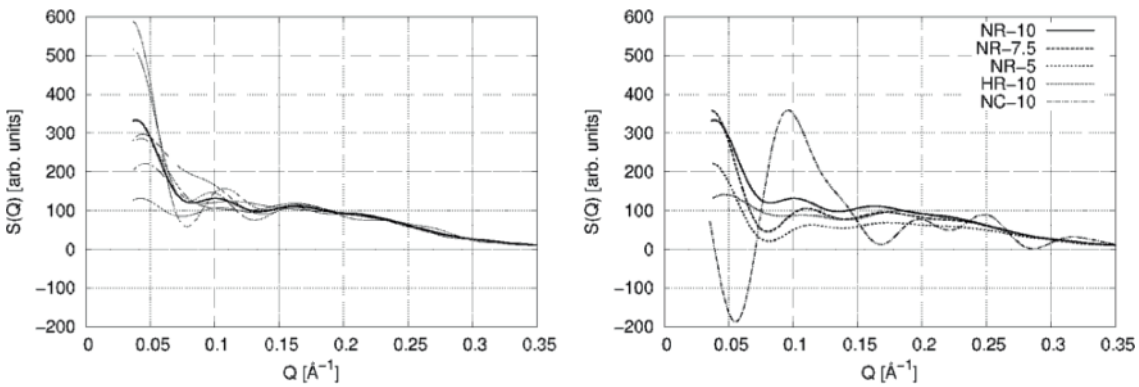

Fig. 3. X-ray weighted $S(Q)$, computed from the last configurations for all systems. Left panel: the various NR-10 runs (thin lines, see Tab. 1) and their average (fat line); right panel: the averages over equivalent systems from Table 1.

appears in all cases. Note that the diverging values at the lowest Q are due to the fluctuating volumes in the NpT-simulations. The feature around 0.1 Å^{-1} is shifted to lower Q-values when increasing the water content, as in the experiments [4, 5, 63, 64]. Furthermore, all the curves decay smoothly to zero at large Q-values, as described above for the Porod region. Hence, all our systems can be considered as possible conformations of real Nafion.

The ionomer peak for the cylinder configuration NC-10-1 is found at a slightly lower Q-value than for the other systems. The average spacing between the aqueous domains is thus larger here. On the other hand, the position of this peak for the Hyflon systems (HR-10-1, HR-10-2) is in the same Q-range as that of the other Nafion systems, no significant difference can be detected.

5.2. Cluster Analysis

We have investigated the aggregation and the size distribution of the aqueous domains using standard [67] and modified [53] cluster analyses. The spatial distribution of a given kind of particle was discretized into clusters according to a distance criterion. We considered here only the water oxygen (Ow) atoms and the K^+-ions. We chose as the criterion for considering two particles as being members of the same cluster the distance at which the radial pair distribution function $g_{\mathrm{Ow-Ow}}(r)$ curve has its first minimum, i. e. 3.5 Å (see [53]). This value was also used by Devanathan et al. [17] to determine the water percolation threshold.

We found again no significant differences in the cluster-size distributions between the NR-10 systems, thus confirming their equivalence. The NR and HR systems are also very similar in this respect, see Figure 4; we thus show only the curve for the systems labeled 1 in Table 1. About 40 aqueous clusters of different sizes were found: among these clusters, one contains almost all ($\approx 99\%$) atoms (peaks on the right of Fig. 4). This is at variance with the work of Cui et al. [68, 69] who observed a less dispersed water distribution in Nafion as compared to Hyflon.

The cylindrical system showed a significantly larger number of clusters, about 100, with a different distribution of the small ones, see Figure 5. However, almost all (more than 98%) atoms were in one dominant cluster. The figure shows that clusters containing 10 to 20

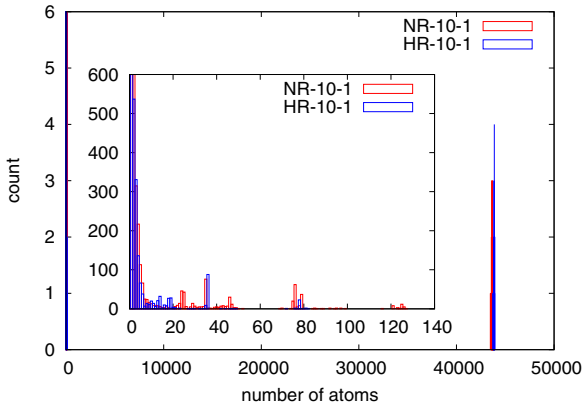

Fig. 4 (colour online). Histogram of the number of clusters with a given number of atoms in the NR-10-1 and HR-10-1 systems, accumulated every 100 ps over 10 ns, hence for 100 configurations. Only Ow-atoms and K^+-ions are considered; the distance criterion is 3.5 Å. The insert shows a zoom at small numbers of atoms.

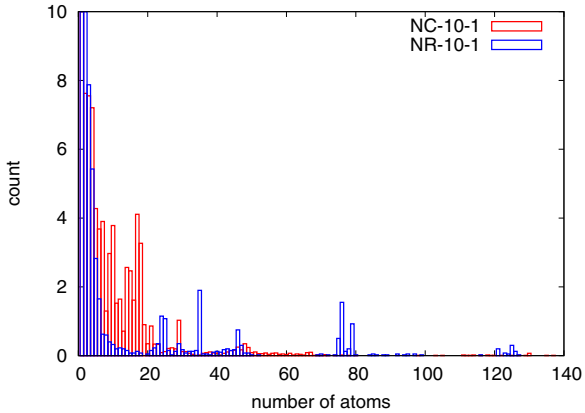

Fig. 5 (colour online). Histogram of the number of clusters with a given number of atoms in the NC-10-1 and NR-10-1 systems, computed as in Figure 4. For comparison, the histograms are normalized by the total number of clusters in each system.

water molecules seem to be more stable in the cylindrical system. We also note that for both morphologies we observed the beginning of the aggregation of the largest cluster from the very beginning of the equilibration procedure, i. e. within about 0.1 ns.

The effect of changing the distance criterion was also examined: $d = 3.0$ and 5.0 Å, below and above the reference value. With $d = 3.0$ Å, the number of clusters increased from roughly 40 to roughly 2700 – 2800, and the population of the largest cluster consequently decreased to roughly 75 – 80%. With $d = 5.0$ Å, the

number of clusters decayed to roughly 5 and the largest cluster became even more dominant. Since we do not expect a polymer chain to be present between aqueous clusters separated by about (5.0 – 3.5) Å = 1.5 Å, we conclude that the small clusters must be located at the periphery of the dominant one.

Decreasing the water content λ leads to smaller largest clusters and to an increased number of clusters. Typically, roughly 65 and 140 clusters were found for the NR-7.5 and NR-5 systems, respectively, with the dominant cluster containing $\approx 98\%$ and 94% of the water molecules and ions. Water percolation is thus probable in all systems hydrated at $\lambda \gtrsim 5$; the threshold must thus occur below this value, i. e. below the $\lambda = 5-6$ range predicted by Devanathan et al. [17]. Malek et al. [70], on the other hand, predicted a value of $\lambda = 4$.

Since a very large and dominant cluster was observed in all cases, we have applied a modified clustering routine to attempt to discretize this cluster into denser subclusters, possibly interconnected by bridges. Atoms with a 'low' coordination number (down to three or two) are iteratively removed from the analysis until dense subclusters emerge, see [53] for details. The largest cluster is subdivided by this procedure into subclusters for all systems, yet the degree of subdivision varies strongly with λ, see Figure 6. There are roughly 20, 40, and 110 subclusters for both the NR-10 and HR-10, the NR-7.5, and the NR-5 systems.

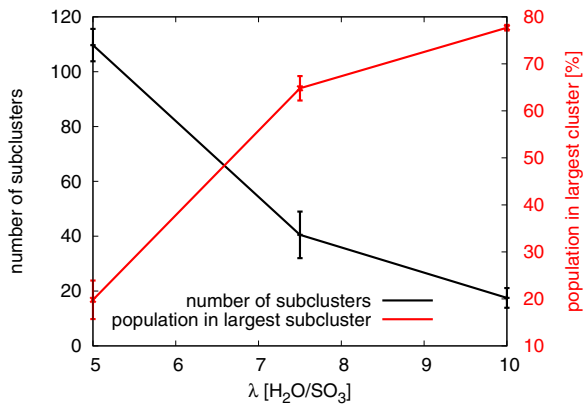

Fig. 6 (colour online). Number of subclusters (in black) and number of atoms (in % of total) in the largest subcluster (in red), after iterative removal of atoms with up to two neighbours, vs. λ, averaged over the last 10 ns of the NR-10 and HR-10 systems, of the NR-7.5, and of the NR-5 systems. The root mean square deviation was used to estimate the error bars.

Among these subclusters, the largest one contains, respectively, about 80%, 65%, and 20% of the total population. Identical values are thus again observed for the NR-10 and HR-10 systems.

6. Dynamics

The self-diffusion of the water molecules and cations in Nafion/Hyflon systems in equilibrium is of particular interest with respect to the process of charge transport. The values obtained here from the mean square displacements for the water molecules are in reasonable agreement with the ones obtained experimentally, e. g., in [71, 72]). They are roughly ten times lower than those obtained for liquid water at room temperature. In contrast to Karo et al. [54], we do no see any significant difference between Nafion and Hyflon systems. A detailed discussion of this as well as of the diffusivity of the other particles is, however, beyond the scope of this first communication.

7. Conclusions and Outlook

This work aims to study the structure of Nafion/Hyflon/water systems at the molecular level and at the nanometer scale. The tool is molecular dynamics (MD) computer simulations. The main difficulties encountered are rooted in the very different time scales involved in the dynamics of the systems. Here we have attempted to overcome these difficulties by a particular choice of initial conditions, which lead to largely unbiased extended polymer chain configurations.

We have obtained several different, but equally plausible configurations for hydrated Nafion/Hyflon/water systems, with different water contents, which lead to scattering functions in equally good agreement with the experimental ones. Such an agreement was also found in most of the large-scale systems studied by Knox and Voth [18]. Since we have attempted to limit the entanglement of the polymer chains when generating the systems, and since the least entangled systems by Knox and Voth also seem to be the ones closest to experiment, one might speculate that this is one key feature leading to the observed features in the scattering experiments, as expressed in the so-called ionomer peak. In contrast to some earlier work [54, 69], we do not observe significant differences between Nafion and Hyflon.

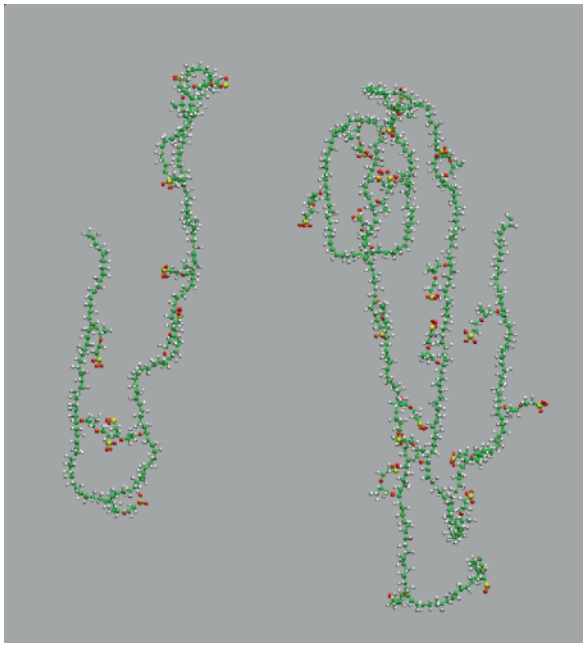

Fig. 7 (colour online). Random growth process of the CF_2-backbones and the side chains of Nafion. Left panel: example of a growing chain; right panel: example of a completed chain. The C-, F-, O-, and S-atoms are shown in green, white, red, and yellow, respectively.

Since both the 'cylindrical' model and the 'random' model proposed here as well as most of Voth's model systems reproduce the experimental scattering data satisfactorily, we must conclude that the scattering data alone are not sufficient to elucidate the structure of systems as complex as proton exchange membranes in water, hence the ongoing debate over their morphology.

The agreement in the scattering functions gives confidence that a more detailed analysis of the so-obtained configurations is warranted. The aggregation and the size distribution of the aqueous domains was thus investigated using clustering algorithms. All systems (Nafion at various λ-values ($\lambda \geq 5$) and morphologies, Hyflon) exhibit a dominant aqueous cluster containing the majority of the water molecules and ions. The size of the largest cluster depends, as it should be, on λ, but not much on the side chain length and the morphology, which is, however, reflected in the distribution of the many smaller clusters. The inhomogeneity of the density in the main cluster, expressed by the number of dense subclusters into which it can be divided, increases by a factor of about 5 when λ goes from 10 to 5.

This work has shown the power and limitations of molecular simulations of complex systems. A wealth of data related to local and some global properties could nevertheless be obtained. However, phenomena with characteristic times longer that the ones attainable in these simulations remain mostly elusive. With some ingeniousness, these shortcomings can be alleviated, as demonstrated here and elsewhere. While proton transport within the aqueous domains of polymer electrolyte membranes is presently understood reasonably well, much more theoretical work is desirable to elucidate those static and dynamical aspects of the polymer morphology which contribute to the performance (or lack of performance) of proton exchange membrane fuel cells.

Acknowledgements

This work is part of GM's doctoral thesis for a joint degree by Universität Duisburg-Essen (UDE) and Université Bordeaux 1. The thesis was defended on July 16, 2012 in Essen. Computer time at the UDE Cray computer operated by the Center for Computational Sciences and Simulations (CCSS) is gratefully acknowledged.

Appendix

Growing the Polymer Chains

A sequence of backbone C-atoms is generated starting from random x, y, z-coordinates inside the volume. Using polar coordinates and a fixed C–C bond length ($r = 1.54$ Å), plus conditions avoiding overlaps (distance between two non-bonded C-atoms > 4.1 Å), the next C-atom is generated. The limiting values for the backbone C–C–C angles are chosen so that a reasonable growth rate is achieved, while i) keeping a reasonable persistence length and ii) allowing turns with a sufficient probability. At the end, each polymer chain will contain 20 side chains, periodically separated by 15 CF_2 groups. It has a maximum length of about 19 nm. However, in order to preserve the periodicity (needed for the simulations) in our systems, the linear extension of the polymers must not exceed the linear dimension of the available volume. The chains are thus prevented from growing outside the periodic unit.

Two F-atoms are fixed on each C-atom, with fixed bond lengths and reasonable F–C–C angles. Every 15

such CF_2-groups, we add a pendant side chain. Overlaps involving the side chains are also prevented via a distance criterion. The growth process is illustrated in Figure 7 with a completed and a growing Nafion chain. The effect of adding rigid boundaries on the growth process can be seen: whenever a chain approaches one of the face of the simulation box, it proceeds in a u-turn.

Growing the polymer chains at low densities is not a problem, as the probability for the currently growing chain to overlap with other chains or with itself is low. If it by chance nevertheless happens, there is enough free space in the box to find an alternative random growth path without overlaps. However, the more chains have already been grown, the more likely it will be that the growth process will get stuck. In this case, we shorten the chain by removing monomeric previous sequences (i. e. we remove backbone atoms up to the last side chain). A new growth path, starting from this point, is then attempted. This way of proceeding was found to be adequate to generate random polymer structures without overlaps and at densities below, but close enough to the experimental one. Furthermore, we can easily generate as many different initial structures with identical properties as we wish.

200 polymer chains were thus placed in this way in $20 \times 20 \times 20\,\mathrm{nm}^3$ cubes, leading to a polymer density of about $950\,\mathrm{kg \cdot m^{-3}}$, which is about half the experimental density of dry Nafion. For the Hyflon, a larger $30 \times 30 \times 30\,\mathrm{nm}^3$ cube was used as a test, even though, with the shorter side chains, the problem of entanglement should be less severe. As mentioned above, under identical conditions ($p = 1$ bar, $T = 300$ K), a longer equilibration phase had to be accepted in this case. The 200 chains were first submitted to a standard energy minimization to remove the 'defects' induced by the geometrical construction.

Before adding the water and ions, the polymer was simulated for 0.5 ns in the NpT-ensemble, at room temperature and pressure. The remaining empty volume was then filled with water molecules (for $\lambda = 10$) and as many K^+-ions as there were SO_3^--groups in the box. This led, before equilibration of the hydrated systems, to a density of about $1430\,\mathrm{kg \cdot m^{-3}}$. This is lower than the experimental density ($\approx 1700\,\mathrm{kg \cdot m^{-3}}$ [73]). The type of cation, here K^+ as the SO_3^--counterion is not expected to be of particular importance for the study of the nanoscale morphology [4, 5, 65]. To generate the systems with a lower water content ($\lambda = 7.5$, 5, see Tab. 1), the appropriate number of water molecules was removed, randomly, from the last configurations of simulations of systems hydrated at $\lambda = 10$, see Table 2, and the systems re-equilibrated.

[1] L. U. Schäfer and A. Klemm, Z. Naturforsch. A **31**, 1068 (1976).
[2] K. Heinzinger and P. C. Vogel, Z. Naturforsch. A **29**, 1164 (1974).
[3] K. D. Kreuer, S. J. Paddison, E. Spohr, and M. Schuster, Chem. Rev. **104**, 4637 (2004).
[4] K. A. Mauritz and R. B. Moore, Chem. Rev. **104**, 4535 (2004).
[5] T. D. Gierke, G. E. Munn, and F. C. Wilson, J. Polym. Sci. **19**, 1687 (1981).
[6] K. D. Kreuer, Chem. Mater. **8**, 610 (1996).
[7] O. Savadogo, J. New Mater. Electrochem. Syst. **1**, 47 (1998).
[8] J. Rozière and D. Jones, Annu. Rev. Mater. Res. **33**, 503 (2003).
[9] M. A. Hickner, H. Ghassemi, L. Site, M. P. Y. S. Kim, B. R. Einsla, and J. E. McGrath, Chem. Rev. **104**, 4587 (2004).
[10] M. K. Petersen, F. Wang, N. P. Blake, H. Metiu, and G. A. Voth, J. Phys. Chem. B **109**, 3727 (2005).
[11] P. B. Balbuena, E. J. Lamas, and Y. Wang, Electrochim. Acta **50**, 3788 (2005).
[12] B. Smitha, S. Sridhar, and A. Khan, J. Membr. Sci. **259**, 10 (2005).
[13] M. Schuster, T. Rager, A. Noda, K. D. Kreuer, and J. Maier, Fuel Cells **5**, 355 (2005).
[14] M. A. Hickner and B. S. Pivovar, Fuel Cells **5**, 213 (2005).
[15] S. Gottesfeld and T. A. Zawodzinski, Advances in Electrochemical Science and Engineering, (Eds. R. C. Alkire, H. Gerischer, D. M. Kolb, and C. W. Tobias), vol. 5, Wiley-VCH Verlag GmbH, Weinheim, Germany 2008, pp. 195 – 301.
[16] M. Eikerling, A. A. Kornyshev, and E. Spohr, Fuel Cells, Advances in Polymer Science, (Ed. G. Scherer), Springer, Berlin Heidelberg 2008, pp. 15 – 54.
[17] R. Devanathan, A. Venkatnathan, R. Rousseau, M. Dupuis, T. Frigato, W. Gu, and V. Helms, J. Phys. Chem. B **114**, 13681 (2010).
[18] C. K. Knox and G. A. Voth, J. Phys. Chem. B **114**, 3205 (2010).
[19] F. Shulu and G. A. Voth, J. Phys. Chem. B **115**, 5903 (2011).
[20] D. Seeliger, C. Hartnig, and E. Spohr, Electrochim. Acta **50**, 4234 (2005).

[21] M. K. Petersen and G. A. Voth, J. Phys. Chem. B **110**, 18594 (2006).
[22] A. Roudgar, S. P. Narasimachary, and M. Eikerling, J. Phys. Chem. B **110**, 20469 (2006).
[23] S. P. Narasimachary, A. Roudgar, and M. H. Eikerling, Electrochim. Acta **53**, 6920 (2008).
[24] A. Roudgar, S. P. Narasimachary, and M. Eikerling, Chem. Phys. Lett. **457**, 337 (2008).
[25] D. Wu, S. J. Paddison, J. A. Elliott, and S. J. Hamrock, Langmuir **26**, 14308 (2010).
[26] S. J. P. Bradley, F. Habenicht, and M. E. Tuckerman, Phys. Chem. Chem. Phys. **12**, 8728 (2010).
[27] R. L. Hayes, S. J. Paddison, and M. E. Tuckerman, J. Phys. Chem. A **115**, 6112 (2011).
[28] M. A. Ilhan and E. Spohr, J. Phys. Condens. Matter **23**, 234104 (2011).
[29] M. A. Ilhan and E. Spohr, J. Electroanal. Chem. **660**, 347 (2011).
[30] C. J. T. de Grotthuss, Ann. Chim. **58**, 54 (1806).
[31] N. Agmon, Chem. Phys. Lett. **244**, 456 (1995).
[32] D. Marx, Chem. Phys. Chem. **7**, 1848 (2006).
[33] G. A. Voth, Acc. Chem. Res. **39**, 143 (2006).
[34] K. Schmidt-Rohr and Q. Chen, Nature Materials **7**, 75 (2008).
[35] R. Devanathan, A. Venkatnathan, and M. Dupuis, J. Phys. Chem. B **111**, 8069 (2007).
[36] R. Devanathan, A. Venkatnathan, and M. Dupuis, J. Phys. Chem. B **111**, 13006 (2007).
[37] N. P. Blake, M. K. Petersen, G. A. Voth, and H. Metiu, J. Phys. Chem. B **109**, 24244 (2005).
[38] M. K. Petersen, A. J. Hatt, and G. A. Voth, J. Phys. Chem. B **112**, 7754 (2008).
[39] A. Vishynakov and A. V. Neimark, J. Phys. Chem. B **105**, 9586 (2001).
[40] A. Vishnyakov and A. V. Neimark, J. Phys. Chem. B **104**, 4471 (2000).
[41] A. Vishynakov and A. V. Neimark, J. Phys. Chem. B **105**, 7830 (2001).
[42] P. G. Khalatur, S. K. Talitskikh, and A. R. Khokhlov, Macromol. Theo. Simul. **11**, 566 (2002).
[43] D. A. Mologin, P. G. Khalatur, and A. R. Khokhlov, Macromol. Theo. Simul. **11**, 587 (2002).
[44] S. Yamamoto and S. Hyodo, Polym. J. **35**, 519 (2003).
[45] J. T. Wescott, Y. Qi, L. Subramanian, and T. W. Capehart, J. Phys. Chem. **124**, 134702 (2006).
[46] D. Wu, S. J. Paddison, and J. A. Elliott, Energy Environ. Sci. **1**, 284 (2008).
[47] D. Wu, S. J. Paddison, J. A. Elliott, and S. J. Hamrock, Langmuir **26**, 14308 (2010).
[48] J. A. Elliott, D. Wu, S. J. Paddison, and R. B. Moore, Soft Matter **7**, 6820 (2011).
[49] S. S. Jang, V. Molinero, T. Çağin, and W. A. Goddard III, J. Phys. Chem. B **108**, 3149 (2004).
[50] H. J. C. Berendsen, J. P. M. Postma, W. F. van Gunsteren, and J. Hermann, in: Intermolecular Forces, (Ed. B. Pullman), Reidel, Dordrecht 1981, pp. 331 – 342.
[51] E. Spohr, P. Commer, and A. A. Kornyshev, J. Phys. Chem. B **106**, 10560 (2002).
[52] G. A. Kaminski, R. A. Friesner, J. Tirado-Rives, and W. L. Jorgensen, J. Phys. Chem. B **105**, 6474 (2001).
[53] G. Marchand, PhD thesis, Universität Duisburg-Essen and Université Bordeaux 1, 2012.
[54] J. Karo, A. Aabloo, J. O. Thomas, and D. Brandell, J. Phys. Chem. B **114**, 6056 (2010).
[55] D. Brandell, J. Karo, A. Liivat, and J. O. Thomas, J. Mol. Model. **13**, 1039 (2007).
[56] S. S. Jang, M. Blanco, W. A. Goddard III, G. Caldwell, and R. B. Ross, Macromol. **36**, 5331 (2003).
[57] S. L. Mayo, B. D. Olafson, and W. A. Goddard III, J. Phys. Chem. B **94**, 8897 (1990).
[58] M. Levitt, J. Phys. Chem. B **101**, 5051 (1997).
[59] B. Hess, C. Kutzner, D. van der Spoel, and E. Lindahl, J. Chem. Theory Comput. **4**, 435 (2008).
[60] H. J. C. Berendsen, J. P. M. Postma, W. F. van Gunsteren, A. DiNola, and J. R. Haak, J. Chem. Phys. **81**, 3684 (1984).
[61] T. Darden, D. York, and L. Pedersen, J. Chem. Phys. **98**, 10089 (1993).
[62] U. Essmann, L. Perera, M. L. Berkowitz, T. Darden, H. Lee, and L. G. Pedersen, J. Chem. Phys. **103**, 8577 (1995).
[63] A.-L. Rollet, G. Gebel, J.-P. Simonin, and P. Turq, J. Polym. Sci. **39**, 548 (2001).
[64] L. Rubatat, A.-L. Rollet, G. Gebel, and O. Diat, Macromol. **35**, 4050 (2002).
[65] E. J. Roche, M. Pineri, R. Duplessix, and A. M. Levelut, J. Polym. Sci. **19**, 1 (1981).
[66] E. J. Roche, M. Pineri, and R. Duplessix, J. Polym. Sci. **20**, 107 (1982).
[67] M. P. Allen and D. J. Tildesley, Computer Simulation of Liquids, Oxford University Press, Oxford 1987.
[68] S. Cui, J. Liu, M. E. Selvan, D. J. Keffer, and W. V. Steele, J. Phys. Chem. B **111**, 2208 (2007).
[69] S. Cui, J. Liu, M. E. Selvan, S. J. Paddison, D. J. Keffer, and B. J. Edwards, J. Phys. Chem. B **112**, 13273 (2008).
[70] K. Malek, M. Eikerling, Q. Wang, Z. Liu, S. Otsuka, K. Akizuki, and M. Abe, J. Phys. Chem. **129**, 204702 (2008).
[71] T. A. Zawodzinski, J. Davey, J. Valerio, and S. Gottesfeld, Electrochim. Acta **40**, 297 (1995).
[72] S. C. Yeo and A. Eisenberg, J. Appl. Polym. Sci. **21**, 875 (1977).
[73] D. R. Morris and X. Sun, J. Appl. Polym. Sci. **50**, 1445 (1993).